Combinatorial alloy design: Renaissance in the accelerated development of high entropy alloys

M. Sadhasivam, Pavan Kumar, Mainak Saha, Chinmoy Mahata, K. G. Pradeep

Correlative Microscopy Lab, Department of Metallurgical and Materials Engineering, Indian Institute of Technology Madras, Chennai - 600036

Abstract:

Combinatorial alloy design - an economical yet high throughput alloy design approach, facilitating rapid screening of a wide range of compositions with limited materials expenditure. The ever-growing demand for multi-functional modern materials necessitates the design of multicomponent alloys that can cater to the requirements of end application, with targeted properties and ease of synthesis. To this end, we report the current trends in combinatorial alloy design approach that are available to develop a subset of multi-component alloys namely, High Entropy Alloy (HEA) in both functionally tailored thin film form as well as in compositionally optimized bulk scale. The thin film form synthesized by combinatorial magnetron sputtering approach enables generation of a composition library in a single-step process, i.e. generating multiple concentration gradients in a single reference substrate. While the identified, best performing compositions from the combinatorial library can then be scaled-up to bulk form utilizing combinatorial vacuum induction melting route for application-oriented design and analysis. As an example, the bulk form of multi-component $Fe_{70-x}Mn_xCo_{10}Cr_{15}Cu_5$ (x=10, 15, 20 at. %) HEA was developed by combinatorial vacuum induction melting route to explore the role of Mn on phase formation and compare them with the theoretical predictions. The hot rolled alloys were subjected to phase analysis by X-Ray Diffraction, microstructure imaging by Scanning Electron Microscopy and chemical composition analysis by Energy Dispersive X-ray spectroscopy towards understanding the role composition on the mechanical property variation in the developed alloys. Such a comprehensive approach would facilitate on the one hand rapid identification of novel, high-performance alloys, while on the other hand support the development of experimentally guided, compositionally tuned materials database for future design of multi-component alloys be it by machine learning or by conventional methods.

1. Introduction

Alloy design is the most crucial requirement from materials' perspective in order to meet the real-time application challenges of any particular system. With the availability of a wide range of traditionally used alloys, the ever-growing demands for novel alloy designs involving multicomponent systems, requires probing of large compositional space. It necessitates the use of high-throughput synthesis and processing methodology which is economically viable and commercially attractive. For instance, if 27 elements are to be considered for the design of an equimolar quinary alloy library, then there would be 81,000 candidates possible and if 40 elements are to be considered, then there would be a possibility of huge library of 658,008 candidates [1]. Therefore, the combinatorial experimental methods have been introduced to accelerate the development of novel multicomponent alloy systems, namely, combinatorial co-deposition of thin-film materials' libraries, diffusion-multiples, laser additive manufacturing, rapid alloy prototyping among others [2, 3]. While the last three approaches are bulk methods which allows for downstream processing and microstructure adaptation, the thin-film method is capable of efficiently synthesizing wider range of compositions. In general, with bulk combinatorial techniques such as rapid alloy prototyping different alloys with tailored compositions along with defined addition of additives can be prepared from a single master melt. Thus, combinatorial synthesis route would enable efficient coupling of alloy development with better compositional accuracy. Further, the exploration of compositional and crystal structure space can be well addressed by combinatorics as intrinsic material characteristics such as phase transformation are essentially dependent on the chemical composition and are more critical than structural properties that are strongly dependent on microstructure for many functional applications. This approach can also be extended to include the effects on the microstructure for the systematically varying alloy compositions [3, 4].

The combinatorial methodology applied via thin film synthesis approach consists of depositing films with widely varying yet systematic composition gradients from multiple sources, most frequently magnetron sputtering sources on a single substrate as shown in Figure 1. The result is the generation of a materials library comprised of gradually changing compositions from the source materials which are then characterized by high-throughput methods for their composition dependent structure and properties. Such a methodology allows in the accelerated screening of compositions towards identifying the champion alloys or at best optimum range of compositions for desired applications. Considering that all the synthesized alloys in a thin film library have been generated at the same time with

the same deposition conditions, the typically observed sample-to-sample variability arising out of multiple sources can be eliminated. However, the obtained phases in this approach are usually metastable and the microstructures are mostly nano-grained and preferentially oriented [4-12].

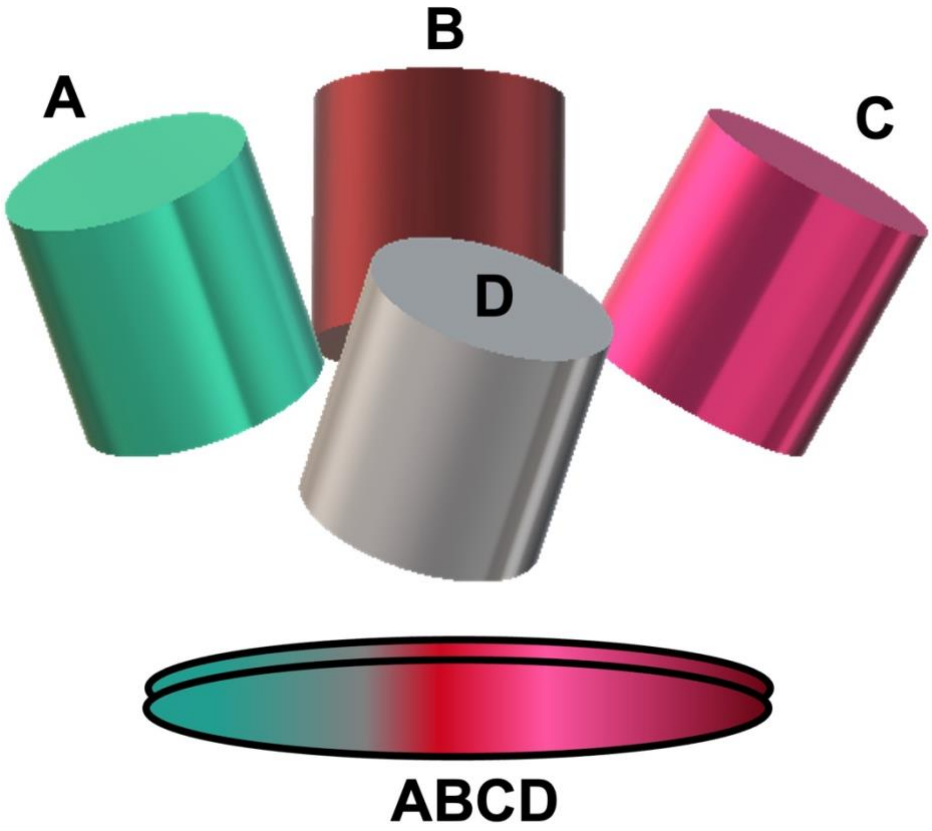

Figure 1. Schematic representation of combinatorial thin film by magnetron sputtering

While developing bulk alloys of specific compositions intended for structural applications, the strength, ductility, toughness etc. are to be measured which in-turn are strongly dependent on the entire thermomechanical history. Hence, microstructure optimization including grain size control, phase formation and distribution are to be considered [13-16]. For the case of transition metal containing alloys, combinatorial Rapid Alloy Prototyping (RAP) approach appears to be suitable. It enables bulk casting of different alloys with well-defined compositions in a single operational step [16]. The

compositional variants that can be achieved in RAP with or without minor additives in bulk form offers the potential of scaling-up to the industrial level.

The field of high entropy alloys (HEA) or compositionally complex alloys (CCA) holds great promise towards introducing novel alloy compositions targeted at special applications due to the promising mechanical properties of the massive solid solution microstructures [5]. The need for high throughput screening of compositions, especially for HEAs/CCAs, has led to the development of experimental approaches such as RAP aimed at accelerated screening of alloys in previously unexplored systems [4, 5]. In this work, we present the near equilibrium, bulk alloy synthesis by RAP based liquid metallurgy route of a non-equiatomic $Fe_{70-x}Mn_xCo_{10}Cr_{15}Cu_5$ (x=10, 15, 20 at %) HEA system thereby enabling comparison with equilibrium thermodynamic calculations and phase predictions.

2. Experimental Methods:

The high entropy combinatorial alloy involving $Fe_{70-x}Mn_xCo_{10}Cr_{15}Cu_5$(x=10, 15, 20 at %) of interest was designed and produced using custom designed vacuum induction melting technique (Inductotherm Pvt Ltd., India) as shown in figure 3. The alloy was developed with the aim to tailor the stacking fault energy (SFE) for exhibiting TRIP along with precipitation strengthening. In this technique, the hot liquid metal can be tapped in multiple water-cooled moulds with defined addition of additives to prepare a tailored range of varying alloy compositions from a single master melt. This method of combinatorial synthesis enables efficient coupling of producing bulk cast alloys with varied compositions along with better compositional accuracy.

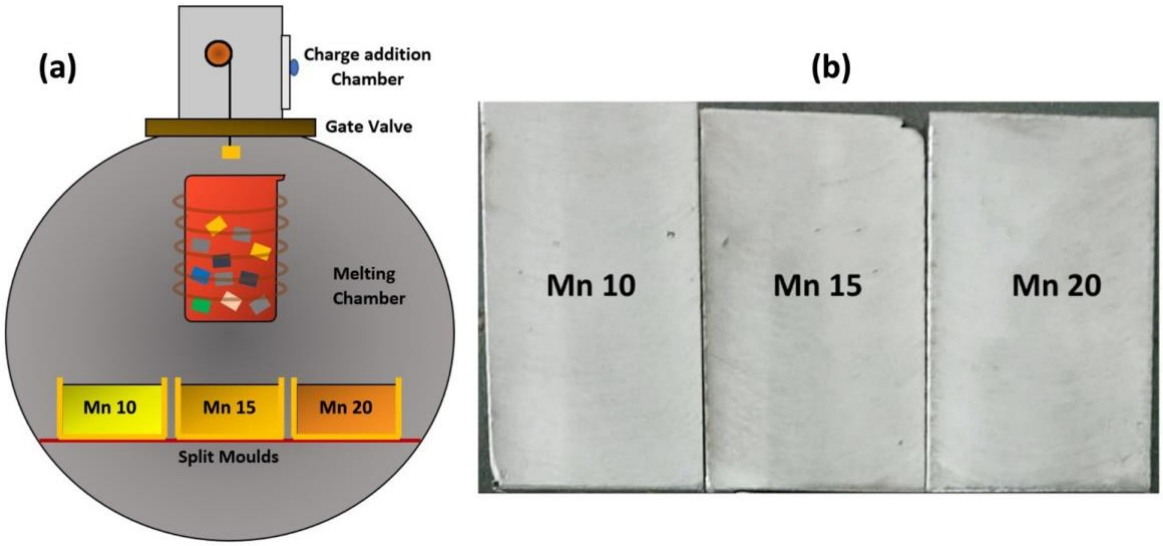

Figure 3 (a) Schematic representation of combinatorial casting
(b) Combinatorially cast blocks with Mn variant (Mn 10, Mn 15, Mn 20)

The produced alloy variants were hot rolled at 950°C to 60% thickness reduction to remove cast heterogeneities. After hot-rolling the alloys were subjected to homogenization annealing at 1200°C for 2 hours followed by water quenching. The homogenized alloys were subjected to X-ray diffraction (XRD) analysis for phase identification. XRD was carried out in a X'Pert PRO, PANalytical instrument with Cu K_α radiation, (λ= 0.154 nm) and a step size of 0.02˚. Optical microscopy (OM), Scanning electron microscopy (SEM), and energy-dispersive X-ray spectroscopy (EDS) analyses were carried out to study the microstructure and elemental distribution/homogeneity at the bulk scale. Electron Backscattered Diffraction (EBSD) was performed for orientation mapping and phase analysis. Optical microscopy was carried out using LEICA DM-2700M microscope. The SEM, EDS, EBSD analysis were performed in a FEI-Helios G4 UX dual beam microscope attached with an Octane elect plus EDS detector and Hikari plus EBSD detector. The EBSD data was analysed using TSL-OIM 8 analysis software. Microhardness test was performed to determine the hardness of the HEAs as a function of varying composition, at a load of 500gf with a dwell time of 10s in FALCON 500, Innovatest microhardness tester. Thermodynamic estimations of phase stability were obtained using the TCFE12 database of ThermoCalc software (v2022b).

3. Alloy Design:

The Transformation induced Plasticity (TRIP) exhibiting FCC family of HEAs namely, $Fe_{80-x}Mn_xCo_{10}Cr_{10}$ (x = 30-40 at. %) are often studied because of their unique behavior of exhibiting simultaneous increase in strength and ductility [13]. Typically, the Twinning Induced Plasticity (TWIP) effect during deformation has been the main mechanism for the good combination of strength and ductility in most FCC based HEAs. Even though the ductility of HEAs is surplus, the ultimate strength (lower than 800 MPa) is not sufficient for structural applications. So, the selected 'x' range of $FeMn_xCoCr$ becomes prominent as it belongs to the limited category of only metastable family in HEAs where TRIP has been observed in addition to TWIP to enhance the mechanical strength [13]. In addition, the presence of precipitates can further strengthen this class of HEAs.

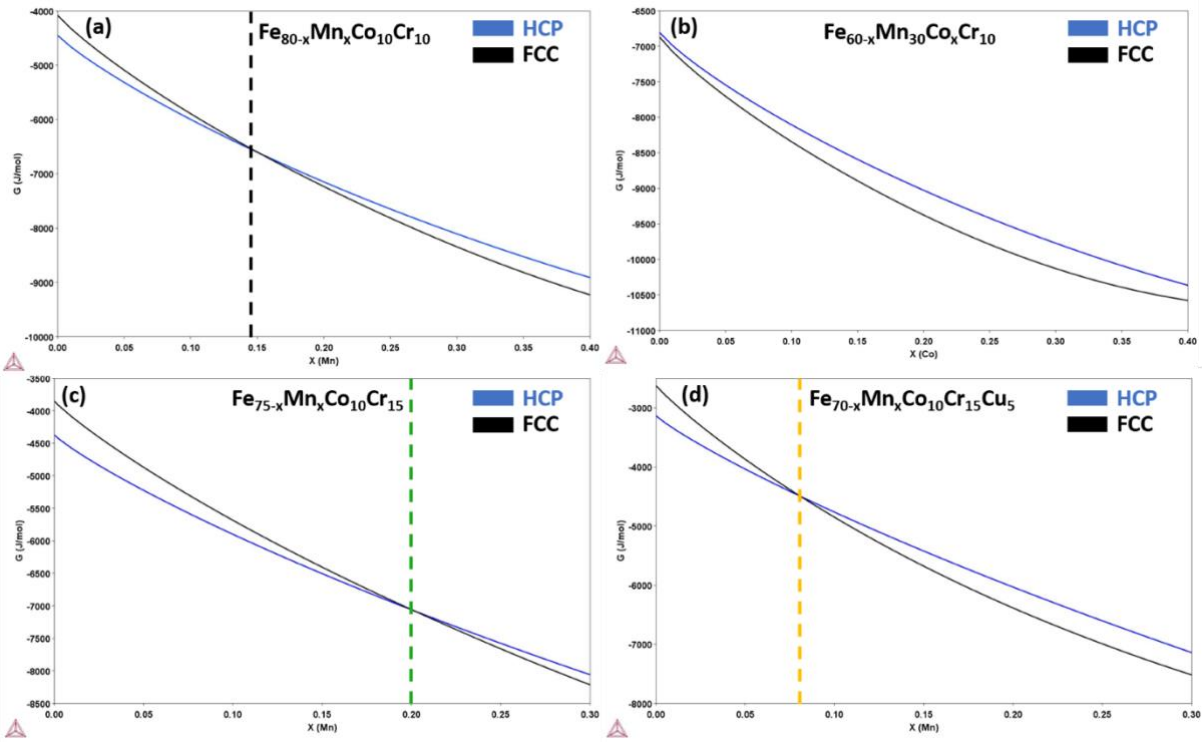

Figure 2. Gibbs free energy (G) vs Composition (X) plot for (a) $Fe_{80-x}Mn_xCo_{10}Cr_{10}$ (b) $Fe_{60-x}Mn_{30}Co_xCr_{10}$ (c) $Fe_{75-x}Mn_xCo_{10}Cr_{15}$ (d) $Fe_{70-x}Mn_xCo_{10}Cr_{15}Cu_5$

For designing the alloy composition, CALPHAD based thermodynamic stability of the two major phases viz. FCC and HCP were predicted for all the constituent alloying elements as shown in Figure 2. The Gibbs free energy vs composition diagram shows the relationship

between the Gibbs free energy (G) for FCC and HCP phases as a function of varying Mn, Co content for the FeMnCoCr HEA along with its variant i.e the Cu alloyed system (to introduce precipitation strengthening). Figure 2(a) and (b) shows the role of varying Mn and Co in FeMnCoCr alloy. The variation in Co has no significant effect in reducing the phase stability of the FCC whereas Mn lowers the free energy at around 15 at.% as can be noticed from the cross-over point. The results for the alloy with slightly higher Cr (15 at.%) without Cu (Fig. 2c) shows a reduced free energy difference between HCP and FCC but the cross-over point is shifted to higher Mn concentration of around 20 at.%. But with the addition of 5 at.% Cu (Fig. 3 d), the cross-over point is shifted to lower Mn concentration at around 8 at.% . Therefore, the FCC family of non-equiatomic FeMnCoCr based HEA with Cu addition shows increased metastability at the narrow region of varying Mn concentration (between 5 to 20 at.%). This necessitates the adaptation of combinatorial methodology to explore this new alloy combination with varying Mn content towards understanding the metastability of FCC leading to combined TRIP and possible precipitation strengthening.

4. Results and Discussions of bulk HEA:

4.1. XRD:

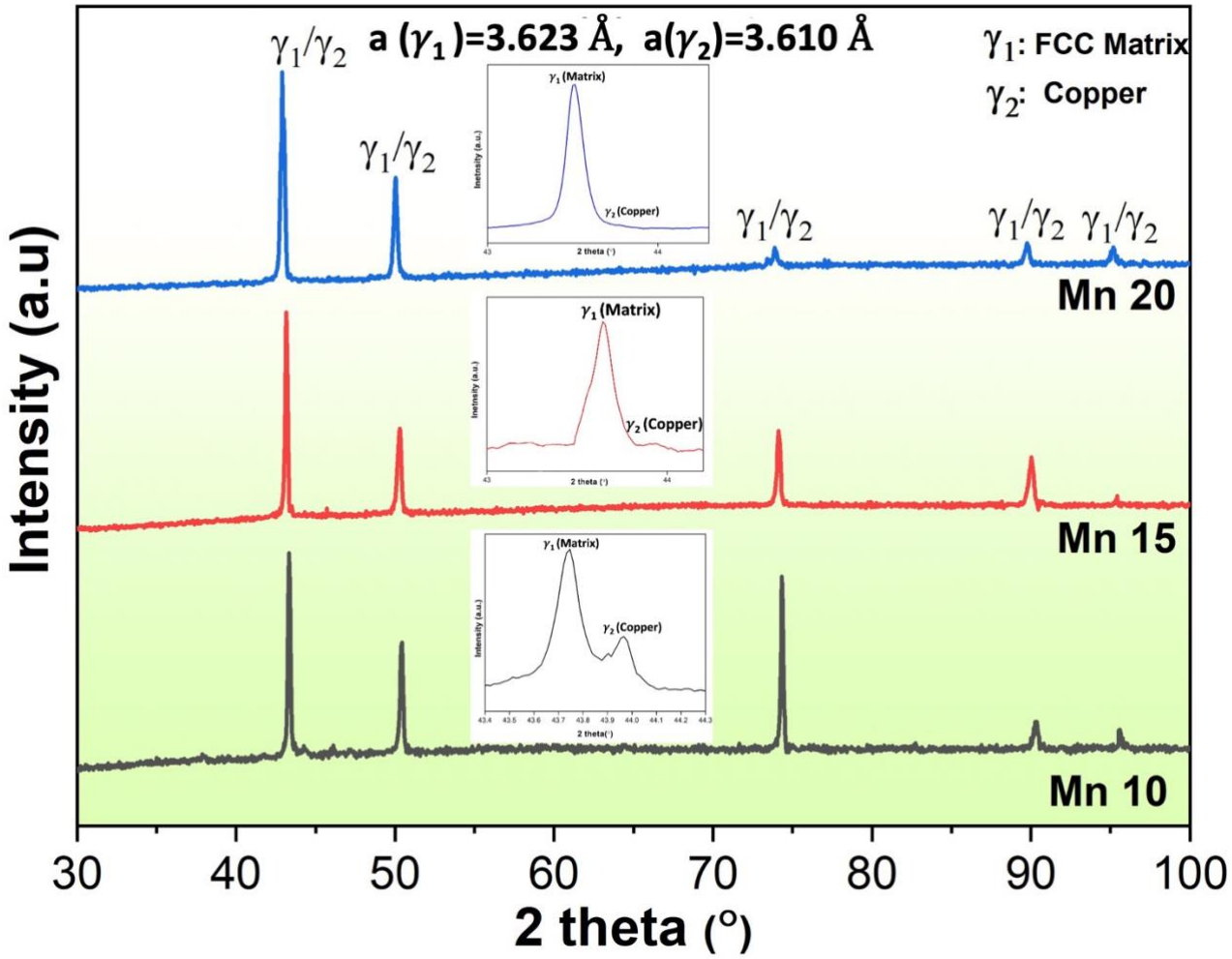

Figure 4. X-Ray Diffractogram of $Fe_{70-x}Mn_xCr_{15}Co_{10}Cu_5$

The X-ray diffraction patterns shown in fig. 4 indicate the presence of FCC phase for all the combinatorially synthesized HEAs with Cu addition. The inset figure (showing enlarged (111) FCC phase peak region) clearly indicates the presence of second FCC phase potentially that of Cu induced minor phase in addition to the matrix FCC peak. It is also noticeable that the volume fraction of the potential Cu rich phase decreases with an increase in the Mn concentration. No other phase peaks, especially those of HCP phase were identified. Also, there is no appreciable texture observed in the FCC phases following hot rolling. The lattice parameter of the FCC matrix phase was determined to be a=3.623Å which was consistent for all three alloying variants whereas the lattice parameter of potential Cu-rich phase was calculated to be 3.610Å.

4.2. Microstructure:

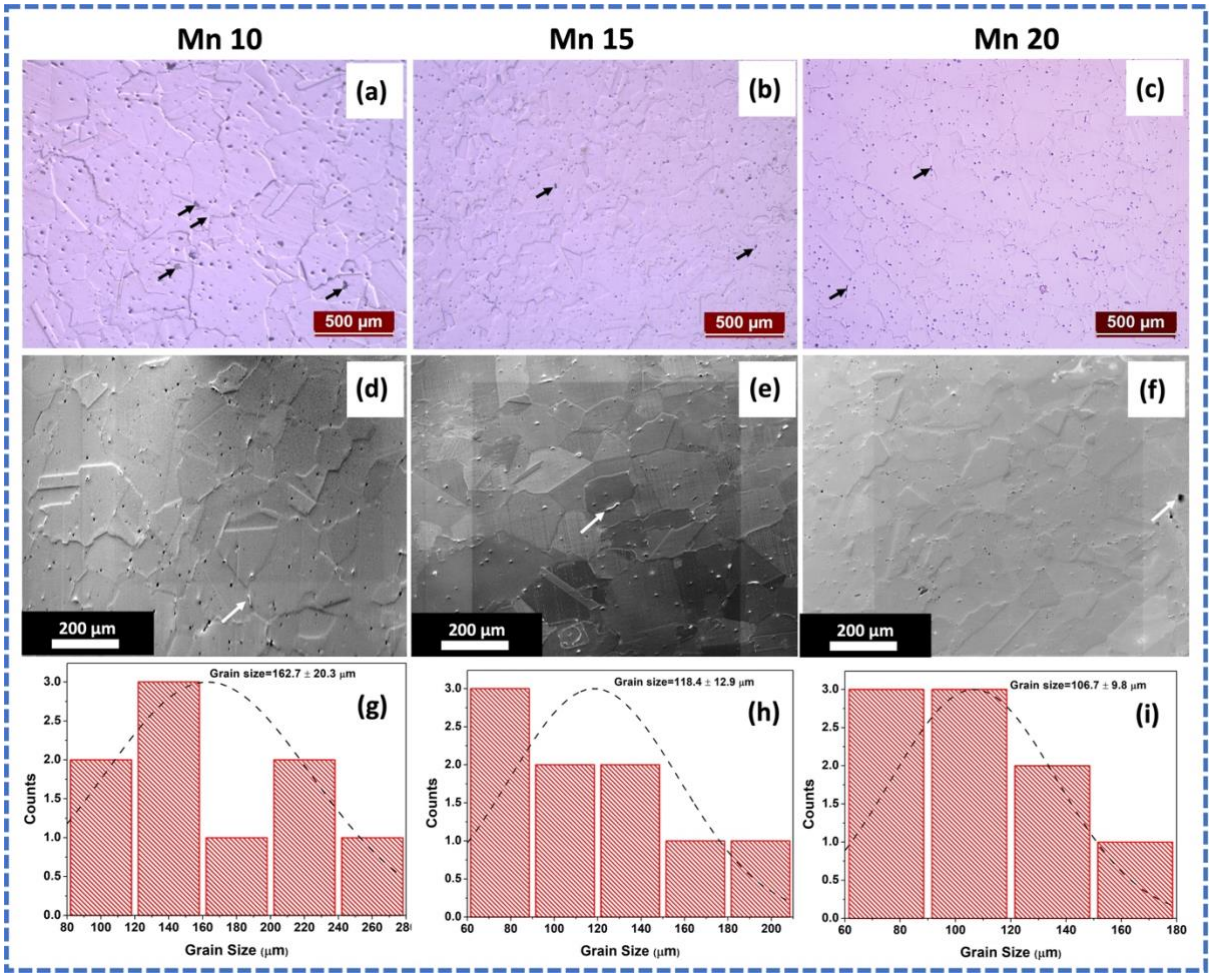

Figure 5. Optical Micrographs of (a) Mn 10 (b) Mn 15 (c) Mn 20; corresponding SEM microstructures of (d) Mn 10 (e) Mn 15 (f) Mn 20; and the Grain size distribution of (g) Mn 10 (h) Mn 15 (i) Mn 20 HEAs.

The optical microstructure reveals the homogeneity in the grain structure without the presence of cast dendrites and any visible defects following hot rolling. The clearly defined grain boundary (GB) region is visible in all the Mn varying HEAs. In addition, the presence of minor second phase precipitates could be noticed (indicated by black arrow), in all the conditions which could likely be the Cu rich FCC phase observed in XRD. The SEM images further reveal the presence of well-defined grains in all the alloys along with the likely Cu rich precipitates as indicated using the arrows. The grains size distribution plot shows the average grain size for Mn 10 alloy is 162.7 ± 20.3 µm whereas the grain size of Mn 15 and Mn 20 HEAs are found to be 118.4 ± 12.9 µm and 106.7 ± 9.8 µm respectively.

To determine the chemistry of the precipitates and the chemical homogeneity of the constituent elements in the matrix, EDS mapping was performed as shown in Fig. 6. The quantitative elemental analysis of all constituent elements is shown in table 1. The obtained chemical composition is comparable to the nominal composition of the targeted combinatorial HEAs. The grain boundary thickening observed in Fig. 6 (a) could be ascribed to the segregation of Mn and Cu along the GBs as can be seen in the concentration profile. The finer globular precipitates in Fig. 6 (a) and (b)are Cu rich while the coarser irregular shaped precipitates in Fig. 6 (c) are constituted by Cu (~ 70 at. %) along with Mn (~ 20 at. %) as given in table 1. The precipitate on which the chemical composition was obtained is encircled in white dashed oval in SEM image of Fig. 6 (a, b, c). The amount of Mn that partitions into the coarser precipitate increases with an increase in the Mn concentration in the matrix. This trend is apparent from the EDS line scan taken across the dotted white arrow as represented in Fig. 6. There is an increase of ~ 50.3% in Mn concentration in the precipitate of Mn 20 variant when compared to the same in Mn 10 variant. The elemental mapping shown in fig. 6 indicates a homogeneous distribution of constituent elements in the matrix region whereas the finer precipitate shows the partitioning of Cu and the coarser irregular shaped precipitate shows segregation of Cu along with Mn. Further investigations are required to determine the exact chemistry and structure details of the precipitates and their evolution.

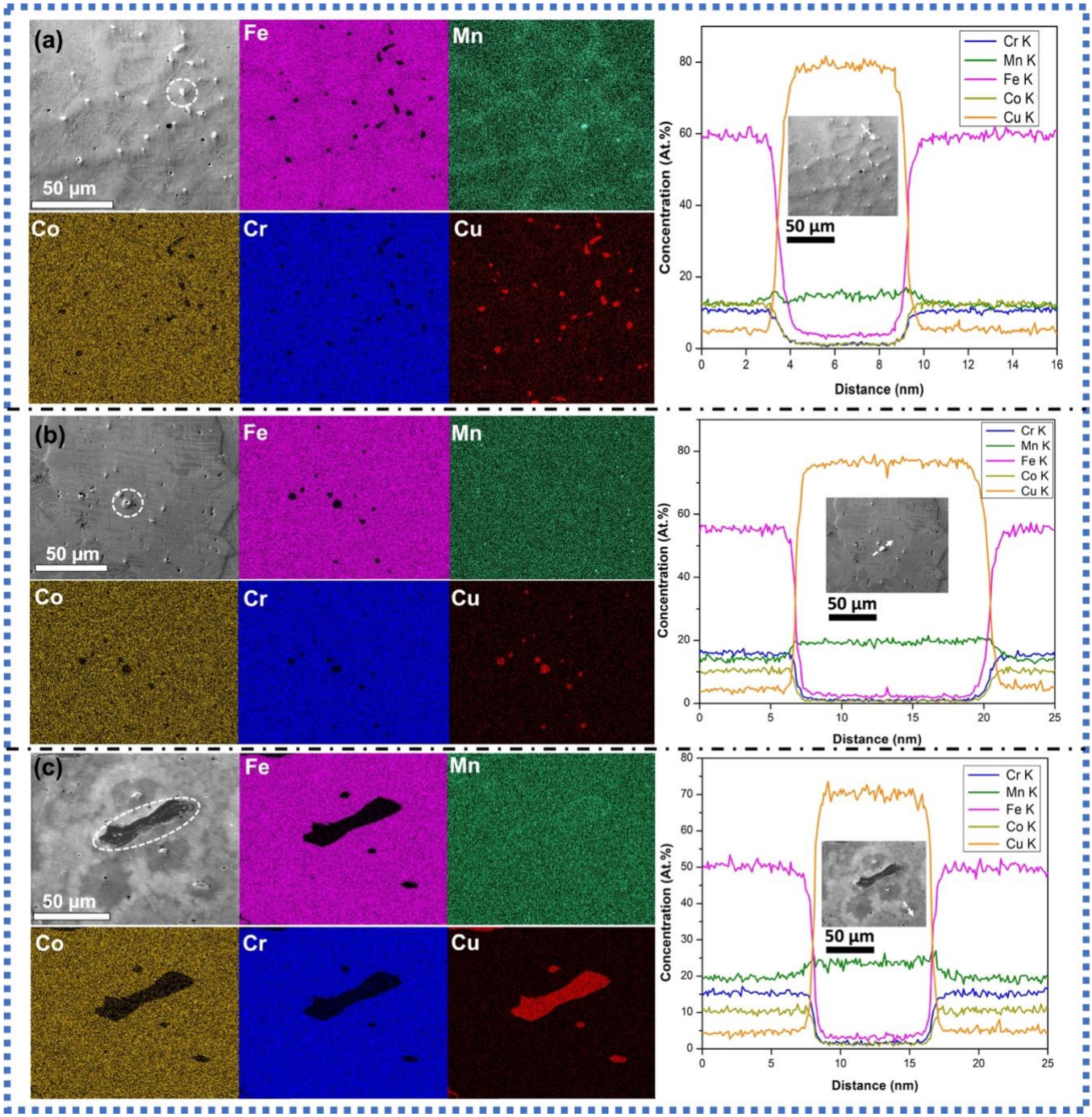

Figure 6. EDS Elemental mapping for (a) Mn 10 (b) Mn 15 (c) Mn 20

Table 1. EDS chemical composition

$Fe_{70-x}Mn_xCr_{15}Co_{10}Cu_5$										
Alloy	**Matrix (Atomic %)**					**Precipitate (Atomic %)**				
	Fe	**Mn**	**Cr**	**Co**	**Cu**	**Fe**	**Mn**	**Cr**	**Co**	**Cu**
Mn 10	59.9± 1.5	10.2± 0.36	15.2± 0.46	10.1± 0.36	4.6±0 .30	4.9± 0.27	18.1± 0.63	1±0. 2	1.4±0 .19	74.7± 1.9

Mn 15	54.7± 1.3	15.8± 0.44	15.6± 0.47	10.1± 0.39	4.7±0 .31	4.3± 0.24	20.8± 0.69	1.7± 0.2	1.1±0 .18	72.1± 1.8
Mn 20	50.9± 1.2	19.4± 0.51	15.4± 0.47	10.1± 0.27	4.7±0 .31	2.9± 0.22	27.2± 0.81	1.3± 0.19	0.9±0 .17	67.7± 2.2

4.3. Electron Backscattered Diffraction (EBSD)

The EBSD results of the three combinatorially synthesized HEAs are shown in figure 7. The inverse pole figure (IPF) map indicates the presence of randomly oriented grains. The average grain size for Mn 10 alloy is ~ 124 µm whereas the grain size of Mn 15 and Mn 20 variants are found to be ~120 µm and ~95 µm respectively. The phase map reveals the presence of a single FCC phase without any traces of HCP in the as-rolled condition. The presence of copper precipitates could not be ascertained due to their near-identical lattice parameter with FCC matrix. In order to understand the effect of applied load on the possible TRIP behaviour in these alloys and their deformation microstructure evolution, a Vickers microhardness test with a load of 500-gram force was applied on the EBSD analyzed area as highlighted by the dotted square in each phase map. EBSD maps taken after indentation revealed the absence of any new phases for all the 3 HEA compositions and hence TRIP appears to have not been activated for the given applied load. The high amount of Cu (5 at.%) in the matrix seem to have increased the stacking fault energy of the system and hence no TRIP effect was realized in all the three HEAs irrespective of varying Mn content. Even though phase separation of Cu in this rolled condition is apparent, the observed precipitate fraction seems to be not significant enough to attract all Cu from the matrix and hence the probable reduction in SFE.

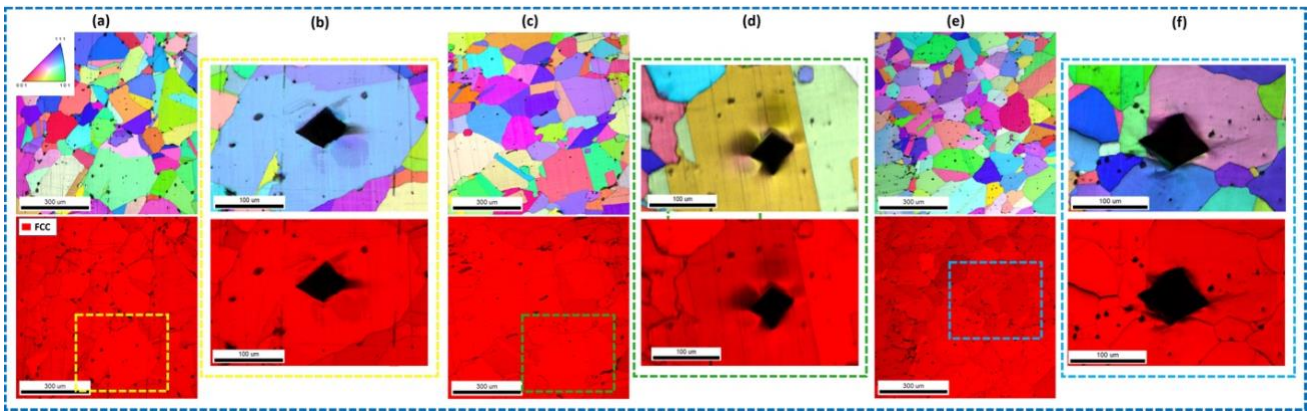

Figure 7. EBSD IPF and Phase maps (a & b) Mn 10 (c & d) Mn 15 (e & f) Mn 20,

4.4. Microhardness

The microhardness results shown in figure 8 indicate an increase in hardness of the alloy with the increase in Mn content with Mn 20 returning the maximum hardness of 231±7 HV. There is a ~25% increase in the hardness for Mn 20 compared to Mn 10 alloy which can be attributed to solid solution strengthening while assuming the Cu rich precipitate fraction to be comparable in all the three HEAs.

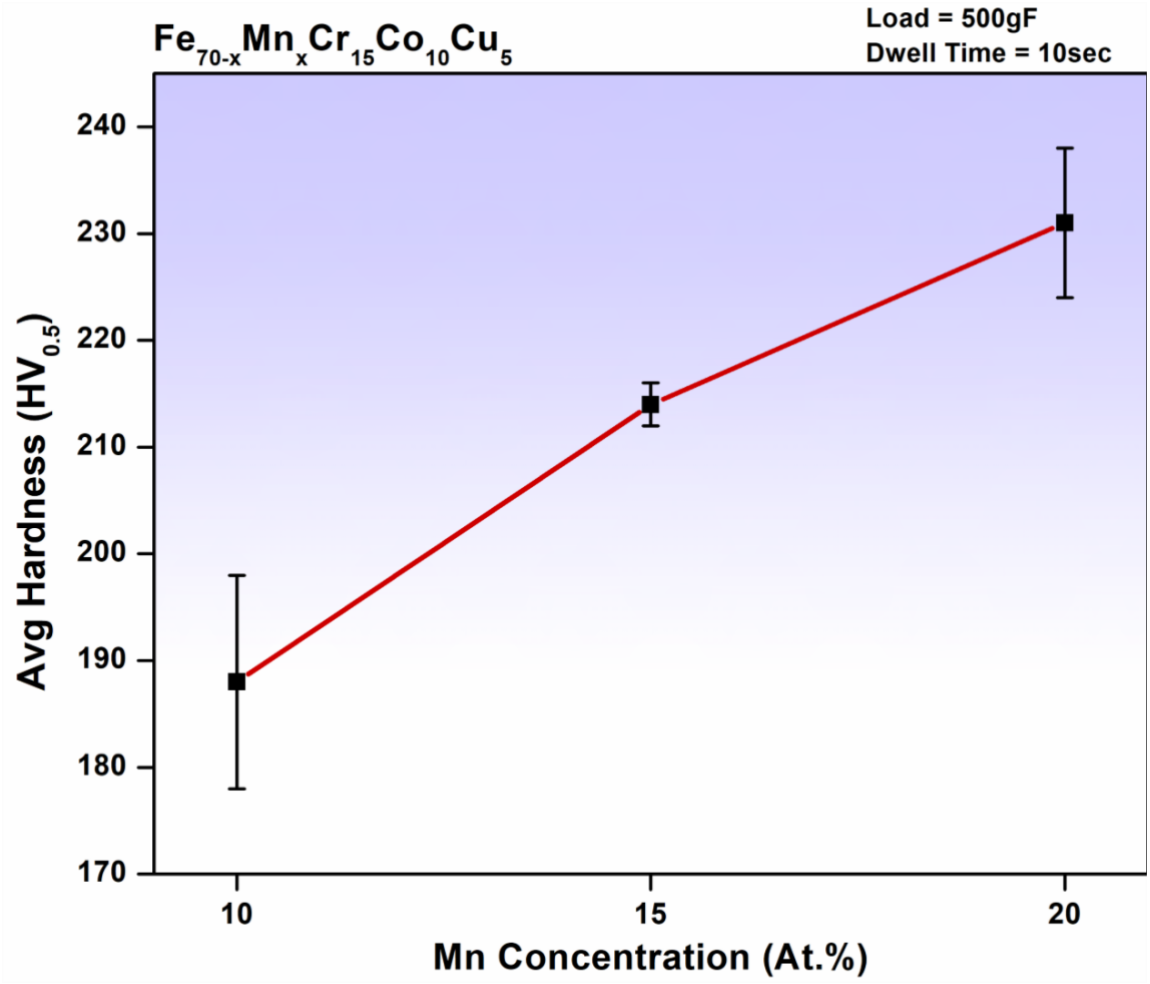

Figure 8. Vickers Microhardness of the alloys

5.5. Solid solution strengthening contribution

Based on the linear dependence model devised by Suzuki and Mott for Fe-based multi-component systems [17], the solid solution strengthening ($\Delta\sigma_{SS}$) may be expressed as:

$$\Delta\sigma_{SS}=K_i C_i \qquad (1)$$

Where, K_i is the solid solution strengthening coefficient for 1 at.% of i^{th} alloying element (solute) and C_i is the concentration (in at.%) of solute 'i' in the solution. Equation (1) is validated for both interstitial and substitutional solutes [18]. In the current series of alloys ($Fe_{70-x}Mn_xCr_{15}Co_{10}Cu_5$ (at.%)), the solutes to be considered for solid solution strengthening contribution of the alloys are Mn, Cr, Co and Cu. For the estimation of $\Delta\sigma_{SS}$ values in these alloys using equation (1), K_i values for Mn, Cr, Co and Cu have been taken as 16.9 [19], 2.6 [19], 2.1 [19] and 50.5 [20] MPa/at.% respectively. Fig. 9 shows the variation of $\Delta\sigma_{SS}$ as a function of Mn content (in at.%). It can clearly be observed that increase in Mn content from 10 to 20 at.% leads to a monotonous increase in $\Delta\sigma_{SS}$ (by ~35%).. The estimated yield strength from Vickers microhardness is also included in Fig. 8 for comparison. Hence, it can be understood that solid solution strengthening is the primary strengthening mechanism in the aforementioned alloys. The possibility of other contributions towards strengthening in the combinatorially designed HEAs require further investigation especially to understand the role of Cu precipitation.

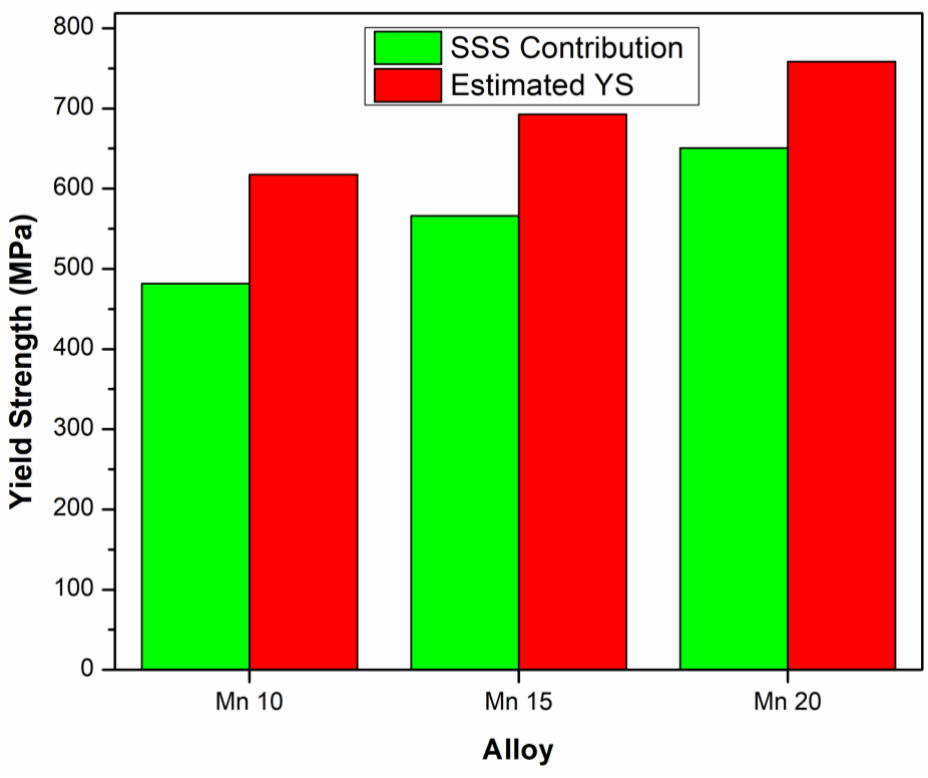

Fig. 9 Solid solution strengthening and Yield strength contribution (in MPa) as a function of Mn content (in At.%) in $Fe_{70-x}Mn_xCr_{15}Co_{10}Cu_5$ alloy.

5. Conclusions

The high-throughput combinatorial alloy design approach for rapid screening of wide range of compositions applicable to the case of multi-component alloys especially the HEAs has been reviewed. The non-equilibrium, thin film form typically synthesized by combinatorial magnetron co-sputtering approach enables generation of a composition library in a single-step process. On the contrary the rapid alloy prototyping approach enables in the production of bulk multi-component alloys with well-defined compositions in reasonable compositional accuracy facilitating comprehensive composition-structure-property analysis under equilibrium conditions. As a case study, the multi-component $Fe_{70-x}Mn_xCo_{10}Cr_{15}Cu_5$ (x=10, 15, 20 at %) HEA was produced using custom designed combinatorial vacuum induction melting furnace to explore the role of Mn on phase formation and compare them with the theoretical predictions. The hot rolled alloys were subjected to microstructural characterization and local hardness measurements. The results indicated that the alloys fabricated were free from significant casting defects and the final composition achieved was the desired nominal composition without appreciable loss of Mn which is possible in such alloys. Among the 3 combinatorially developed variants, Mn 20 showed better hardness (231±7 HV) compared to the other 2 alloys with SSS being the primary strengthening mechanism. Thus, the combinatorial alloy design approach facilitates rapid development of novel, high-performance alloys which can therefore be utilized for future applications.

References:

[1] Wei Chen, Antoine Hilhorst, Georgios Bokas, Stéphane Gorsse, Pascal J. Jacques & Geoffroy Hautier, Nature Communications14, 2856 (2023)

[2] Volker Schnabel, Mathias K€ohler, Simon Evertz, Jana Gamcova, Jozef Bednarcik, Denis Music, Dierk Raabe, Jochen M. Schneider, Acta Materialia 107 (2016) 213-219.

[3] Zhiming Li, Alfred Ludwig, Alan Savan, Hauke Springer & Dierk Raabe, Journal of Materials Research 33, (2018) 3156–3169

[4] Lin Shang, Pradeep Konda Gokuldoss, Stefanie Sandlöbes, Moritzto Baben, Jochen M.Schneider, Journal of the European Ceramic Society 17 (4) (2016) 1339-1347.

[5] K. G. Pradeep, K. Chang, A. Kovács, S. Sen, A. Marshal, René de Kloe, R. E.Dunin-Borkowski & J. M. Schneider, Materials Research Letters, 7:5 (2019) 180-187.

[6] Lin Shang, Moritzto Baben, Konda Gokuldoss Pradeep, Stefanie Sandlöbes , Marshal Amalraj, MarcusHans, Keke Chang, Denis Music, Daniel Primetzhofer, Jochen M.Schneider, Journal of the European Ceramic Society 37 (2017) 35–41.

[7] A. Marshal, K.G. Pradeep, D. Music, L.Wang, O. Petracic & J. M. Schneider, Scientific Reports (2019) 9:7864

[8] Silas Wolff-Goodrich, Amalraj Marshal, K.G. Pradeep, Gerhard Dehm, Jochen M. Schneider, Christian H. Liebscher, Journal of Alloys and Compounds 853 (2021) 156111.

[9] A. Marshal, K.G. Pradeep, D. Music, S. Zaefferer, P.S. De, J.M. Schneider, Journal of Alloys and Compounds 691 (2017) 683-689.

[10] Ludwig, A. npj Computational Materials 5, 70 (2019).

[11] Jun Cui, Yong S. Chu, Olugbenga O. Famodu, Yasubumi Furuya, Jae. Hattrick-Simpers, Richard D. James, Alfred Ludwig, Sigurd Thienhaus, Manfred Wuttig, Zhiyong Zhang & Ichiro Takeuchi, Nature Materials 5, 286–290 (2006).

[12] A Ludwig, J Cao, J Brugger, I Takeuchi, Measurement Science and Technology, 16 111 (2005).

[13] Li, Z., Pradeep, K., Deng, Y. et al. Nature 534 (2016) 227–230.

[14] Y. Deng, C.C. Tasan, K.G. Pradeep, H. Springe, A. Kostka, D. Raabe, Acta Materialia 94 (2015) 124-133.

[15] Zhiming Li, Cemal Cem Tasan, Konda Gokuldoss Pradeep, Dierk Raabe, Acta Materialia 131 (2015) 323-335.

[16] K.G. Pradeep, C.C. Tasan, M.J. Yao, Y. Deng, H. Springer, D. Raabe, Materials Science and Engineering A 648 (2015) 183-192.

[17] R.M. Broudy, Journal of the American Ceramic Society 80 (1958) 5009–5010.

[18] S. Takeuchi, Solid-Solution Strengthening in Single Crystals of Iron Alloys, 27 (2013) 929–940.

[19] Q. Lu, W. Xu, S. Van Der Zwaag, Computational Materials Science 84 (2014) 198–205.

[20] S. Schmauder, C. Kohler, Computational Materials Science 50 (2011) 1238–1243.